ADVANCED MATERIALS

Supporting Information

for *Adv. Mater.*, DOI: 10.1002/adma.201402972

Perylene-Diimide-Based Nanoparticles as Highly Efficient Photoacoustic Agents for Deep Brain Tumor Imaging in Living Mice

*Quli Fan, Kai Cheng, Zhen Yang, Ruiping Zhang, Min Yang, Xiang Hu, Xiaowei Ma, Lihong Bu, Xiaomei Lu, Xiaoxing Xiong, Wei Huang, Heng Zhao, and Zhen Cheng**

Supporting Information

Perylene-Diimide-Based Nanoparticles as Highly Efficient Photoacoustic Agents for Deep Brain Tumor Imaging in Living Mice

*Quli Fan, Kai Cheng, Zhen Yang, Ruiping Zhang, Min Yang, Xiang Hu, Xiaowei Ma, Lihong Bu, Xiaomei Lu, Xiaoxing Xiong, Wei Huang, Heng Zhao, Zhen Cheng**

Experimental Section

Synthesis of PDI

The final **PDI (3)** was synthesized by reaction of its precursor N, N-diisooctyl-1, 7-dibromo-3,4:9,10-tetracarboxylic perylene diimide **(DBrPDI, 2)** with cyclohexylamine. The **DBrPDI** was prepared according to **ref. 1** and **2**. The synthetic routes to target compound are shown in Figure S1. The experimental procedures are given below.

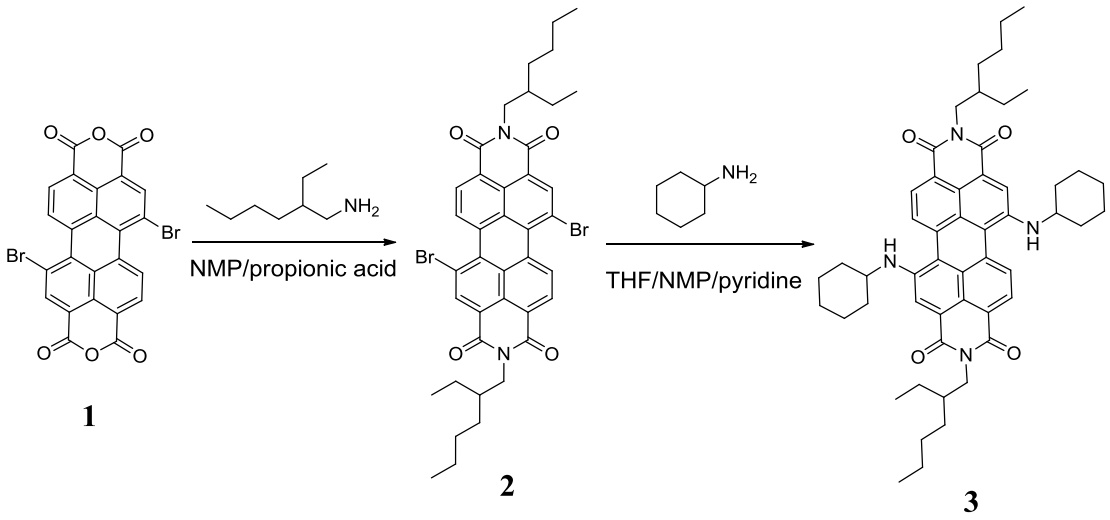

Figure S1. Synthetic route to PDI.

(N, N'-diisooctyl-1, 7-di (cyclohexylamino))perylene-3,4;9,10-tetracarboxy diimide (PDI, 3):

A mixture of **2** (2g, 2.56 mmol) and pyridine (10 mL) was dissolved in N-Methyl-2-pyrrolidinone (150 mL) was stirred under an argon atmosphere. Then, cyclohexylamine (2g, mmol) dissolved in THF (20 mL) was added slowly over 10min. The

reaction mixture was heated to 85°C under nitrogen and then kept at this temperature for 4 days. The reaction mixture was cooled to room temperature, added 50 mL CH_2Cl_2 to the mixture, N-Methyl-2-pyrrolidinone was washed with water (5 × 500 mL) and then dried in a vacuum. The deep green residue was column chromatographed on silica gel with chloroform as eluent. The second green band was collected, and **3** was collected as deep green solid (0.827g, 70%). ^{1}H NMR (300 MHz, $CDCl_3$,TMS):δ= 8.69 (d, 2H), 8.31 (d, 2H), 7.95 (d, 2H), 5.8(s, 2H), 4.10 (t, 4H), 3.68 (m, 2H), 3.5 (br s, 2H), 2.35-1.59 (m, 18H), 1.50-1.17 (m, 20H), 0.87 (t, 12H). ^{13}C NMR (75 MHz, CDCl3, TMS): δ= 164.3, 163.9, 134.1, 130.4, 126.8, 122.6, 122.4, 121.2, 118.6, 116.7, 116.2, 52.1, 44.3, 38.0, 33.3, 30.8, 30.4, 28.8, 25.6, 24.6, 24.1, 23.2, 14.1, 10.7. MALDI-TOF MS (m/z) 808.773, calcd for $C_{52}H_{64}N_4O_4$ (m/z), 808.49. Anal. Calcd for $C_{52}H_{64}N_4O_4$: C, 77.36; H, 7.82; N, 6.90. Found: C, 77.19; H, 7.97; N, 6.92.

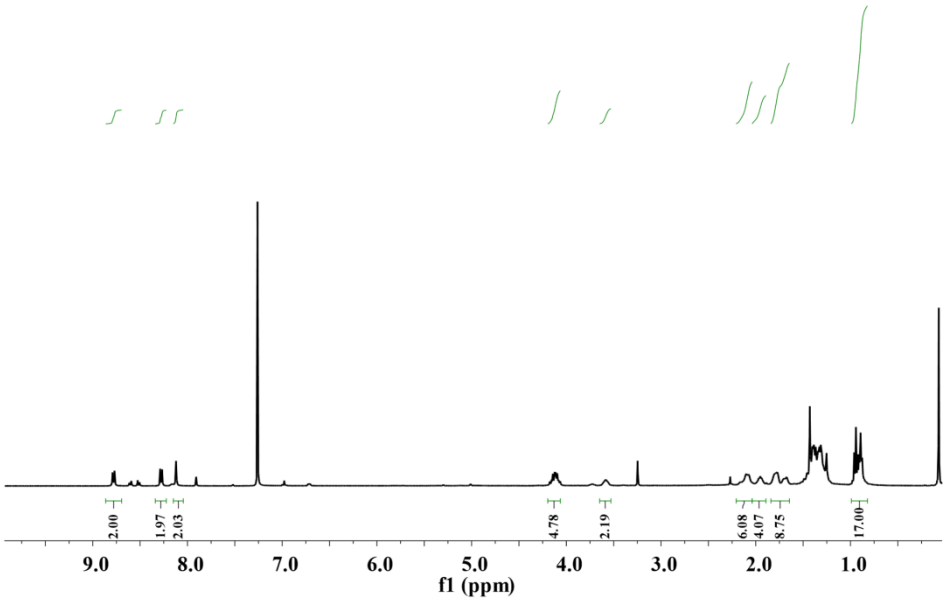

Figure S2. ^{1}H-NMR spectra of 1,7-dicyclohexylamino-substituted PDI.

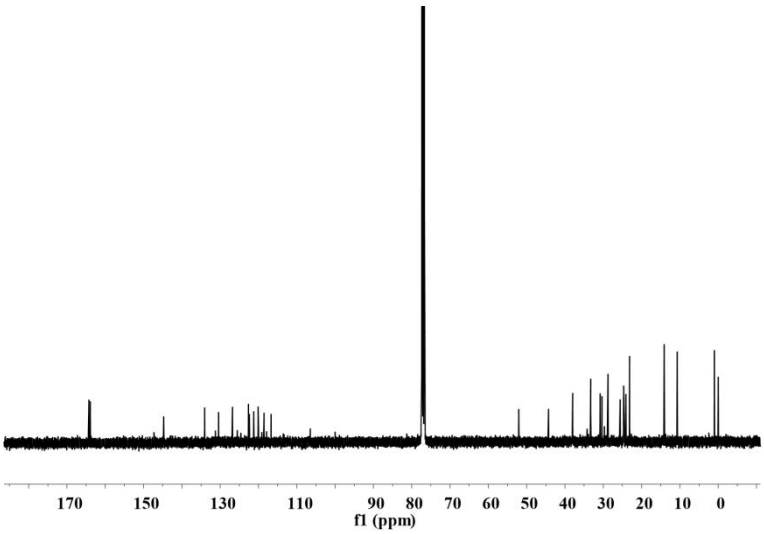

Figure S3. ^{13}C-NMR spectra of 1,7-dicyclohexylamino-substituted PDI.

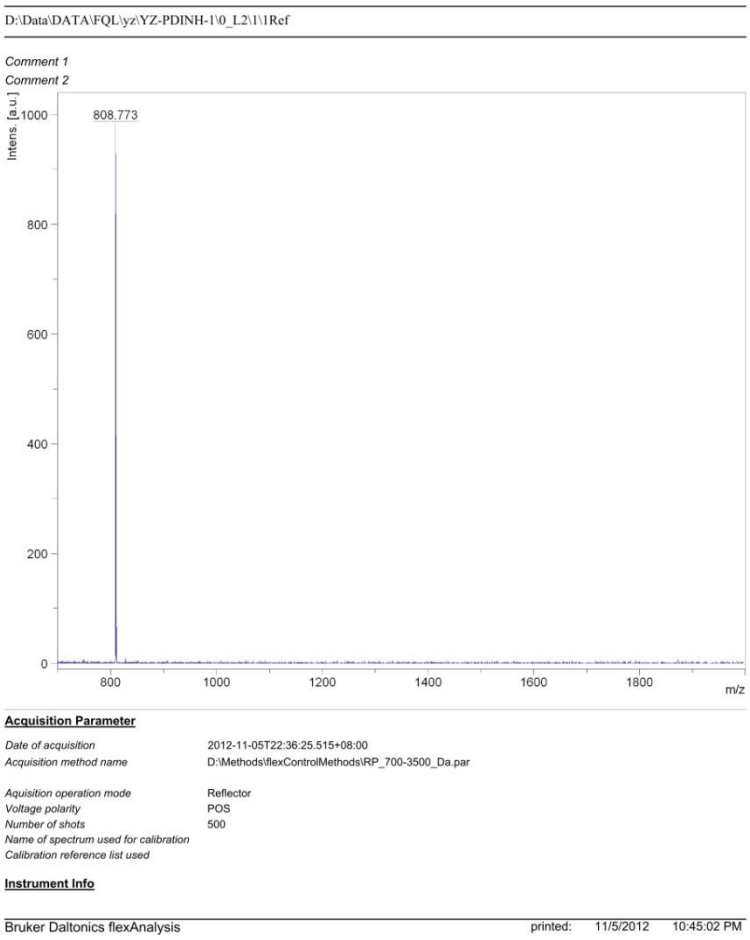

Figure S4. MALDI-TOF spectra of 1,7-dicyclohexylamino-substituted PDI.

Preparation and characterization of water-soluble PDI NPs. PDI (2.0 mg) in 2 mL THF was swiftly dropped into the DSPE-mPEG$_{5000}$ aqueous solution (5.0 mg in 10 mL H_2O) under sonication. THF was then removed by argon blowing on the solution surface under stirring at 40 ^{o}C. A bright green aqueous solution was then obtained. The aqueous solution was further centrifuged with a centrifugal-filter (Amicon centrifugal filter device, MWCO = 100 kDa) and washed with deionized water and repeated several times. The resultant products, PDI NPs, were concentrated by the centrifugal-filter and stored at 4 ^{o}C. The final PDI NPs were reconstituted in PBS and filtered through a 0.22 μm filter for cell and animal experiments. TEM were recorded on a JEOL 2010 transmission electron microscope at an accelerating voltage of 100 kV. The hydrodynamic sizes were measured using dynamic light scattering and zeta potential analyzer (Malvern, Zetasizer Nano ZS90).

The number of PDI molecule in one PDI NP was calculated as follows. Considering the length of PEG (Mw = 5000) was 11.2 nm (**ref. 3**) and the average hydrodynamic size of PDI NP was 53.0 nm, the diameter of the PDI core in PDI NP was about 30 nm. Based on the density of PDI (1.4 g/cm^3), the number of PDI molecule in one PDI NP can be finally calculated to be about 1×10^4. The equation was listed as follows:

$$N_{PDI} = \frac{w_{PDIcore} \cdot N_A}{M_{PDI}} = \frac{V_{PDIcore} \cdot \rho_{PDI} \cdot N_A}{M_{PDI}} = \frac{(4/3)\pi r^3 \cdot \rho_{PDI} \cdot N_A}{M_{PDI}}$$

In this equation, N_{PDI} is the number of PDI molecule in one PDI NP, $w_{PDIcore}$ is the weight of the PDI core in one PDI NP, V_{PDI} is the volume of the PDI core in one PDI NP, M_{PDI} is the molar mass of PDI (808 g/mole), r is the radius of PDIcore (15 nm), ρ is the density of PDI (1.4 g/cm^3), N_A is Avogadro's constant (6.02×10^{23}).

PAI analysis of phantoms. For studying the PAI properties of PDI NPs, a cuboid container was half filled with 1% agarose gel to half depth. Different concentrations of PDI NPs aqueous solutions ranging from 0.15625 nM to 2.5 nM were filled into polyethylene

capillaries and then the capillaries were laid on the surface of solidified agarose gel. The capillaries were further covered with thin 1% agarose gel to make the surface smooth. For the particle's sensitivity in living body, PDI NPs aqueous solutions with different concentrations from 0.625 nM to 20 nM were mixed with matrigel at 0 ^{o}C and then subcutaneously injected on the lower flank of mice. The PAI of the mixtures was performed after they were solidified. PA spectra and PA/US coregistered images were acquired with a LAZR commercial instrument (VevoLAZR; VisualSonics). It is equipped with a LZ-250 linear array transducer and a tunable Nd:YAG laser system (680-970 nm). In our system, the Vevo LAZR PAI System with a laser at excitation wavelength of 700 nm and a focal depth of 10 mm was used to acquire PA and US images. The laser at excited wavelength ranging from 680 nm to 970 nm was sequentially enhanced with a step of 3 nm for the scan of PA spectra. Acquisition rate of 5 frames per second was used for all the experiments. The photoacoustic gain was kept at 42 dB, dynamic range at 18 dB and center frequency of 21 MHz for all studies. US and PA images were obtained sequentially. The PA signals reported were the average pixel intensities from within the Region of Interests (ROIs). Normalization and quantification of the images analysis were carried out using ImageJ.

Orthotopic brain tumor models.

All animal experiments were performed in compliance with the Guidelines for the Care and Use of Research Animals established by the Stanford University Animal Studies Committee. C6 cells expressing firefly luciferase (C6-Fluc) and PBS were inoculated in the brain of female athymic nude mice (two groups, each n =3) in 4–6 weeks old (5×10^3 cells in the striatum: Bregma +1.0 mm, left lateral 2.0 mm, depth 3.0 mm). Detailed process is as follows: While under isoflurane anesthesia the mice were placed in a stereotaxic frame. A sagittal skin incision of 0.5 cm was made on the head and the skull was exposed. A burr hole in the left hemisphere was drilled according to the coordinate 1.0 mm anterior, 2.0 mm lateral to the

bregma. A 10 µl syringe (Hamilton Company, Reno, NV) with a 26-gauge needle (Cat# 80010) was inserted to the striatum and lowered to the depth of 3.0 mm from the dura. C6-Fluc cell (5 µl with 5×10^3 cells) was injected into the striatum over 15 min using a microsyringe pump controller (World Precision Instruments, Inc., Sarasota, FL). The same amount of PBS was also injected as an experimental control, the needle was left for 10 minutes before being withdrawn. The wound was closed and the animals were allowed to recover. The growth of brain tumor was monitored by MRI (using 7.0T MR scanner for T_2 imaging, TR: 4000 ms; TE: 63.2 ms) and BLI. The tumors with the diameter of approximately 2.0 mm and with the depth maxima from 4.5 mm to 4.0 mm (the depth maxima referred to the distances between the nadir of brain tumors and the dura, all detectable by MRI) were used for the next PAI.

PAI of tumor bearing mice *in vivo* and *ex vivo*. Mice bearing brain tumor (C6-Fluc) and PBS were anesthetized with 2% isoflurane in oxygen and placed with prone position. The coronal sections of PA and US imagings were carried out using the Vevo LAZR PAI System as the *in vitro* phantomu study. After 2 days of performing PAI of mice brains *in vivo*, all the blood was drained from the heart and then the brains and other organs were excised and embedded in agarose gel for PAI. Coronal PA and US images of the whole brains and other organ were acquired using the Vevo LAZR PAI System as the *in vitro* phantom study for biodistribution analysis. The PA signals reported were the average pixel intensities from within the Region of Interests (ROIs). Normalization and quantification of the images analysis were carried out using ImageJ. 3D image reconstruction and image analysis were also carried out using ImageJ.

PAI investigation of depth-concentration relationship. The PCR tubes were embedded in a cuboid container filled with 1% agarose gel. After solidification, the tubes were pulled out to

generate holes. Different concentrations of PDI NPs aqueous solutions ranging from 50 nM to 0.390625 nM (50, 25, 12.5, 6.25, 3.125, 1.5625, 0.78125, and 0.390625 nM) suspended in agarose were filled into the holes. The coronal sections of photoacoustic and ultrasound images were then acquired using the Vevo LAZR PAI System as the *in vitro* phantom study. The PA signals reported were the average pixel intensities from within the Region of Interests (ROIs). Normalization and quantification of the images analysis were carried out using ImageJ.

Cell viability. *In vitro* cytotoxicity of PDI NPs was determined in NIH-3T3 cells by the MTT assay. NIH-3T3 cells were incubated on 96-well plate in DMEM medium containing 10% FBS and 1% penicillin/streptomycin at 37 °C in 5% CO_2 humidified atmosphere for 24 h and 0.5×10^4 cells were seeded per well. Cells were then cultured in the medium supplemented with indicated doses of PDI NPs for 24 h. The final concentrations of NPs in the culture medium were fixed at 2.5, 5, 10 and 20 nM in the experiment. Addition of 10 μL of MTT (0.5 mg/mL) solution to each well and incubation for 3 h at 37 °C was followed to produce formazan crystals. Then, the supernatant was removed and the products were lysed with 200 μL of DMSO. The absorbance value was recorded at 590 nm using a microplate reader. The absorbance of the untreated cells was used as a control and its absorbance was as the reference value for calculating 100% cellular viability.

Discussion

Optical properties of PDI dye and its NP

In our system, the absorption and emission spectra of PDI in different organic solvents were shown in **Figure S5-6**. The absorption spectra were dominated by broad and nearly structureless absorption bands that span a large part of the NIR spectrum. The absorption spectra of amino-substituted PDIs were red-shifted along with the increase of the solvent

polarity, such as the maximum absorption of PDIs in ethyl acetate was at 682 nm, and the maximum absorption in dimethyl formamide red-shifted to 704 nm. The fluorescence spectra of PDIs were also largely red-shifted along with the increase of the solvent polarity. These can be attributed to the strong intramolecular charge transfer (ICT) characteristics for both the ground states and excited states of PDI, which were in line with previous reports on the optical properties of amino-substituted PDI (**ref. 4**). Furthermore, PDI showed rather weak fluorescence (ϕ) in different solvents (**Table 1**) due to its strong ICT characteristics.

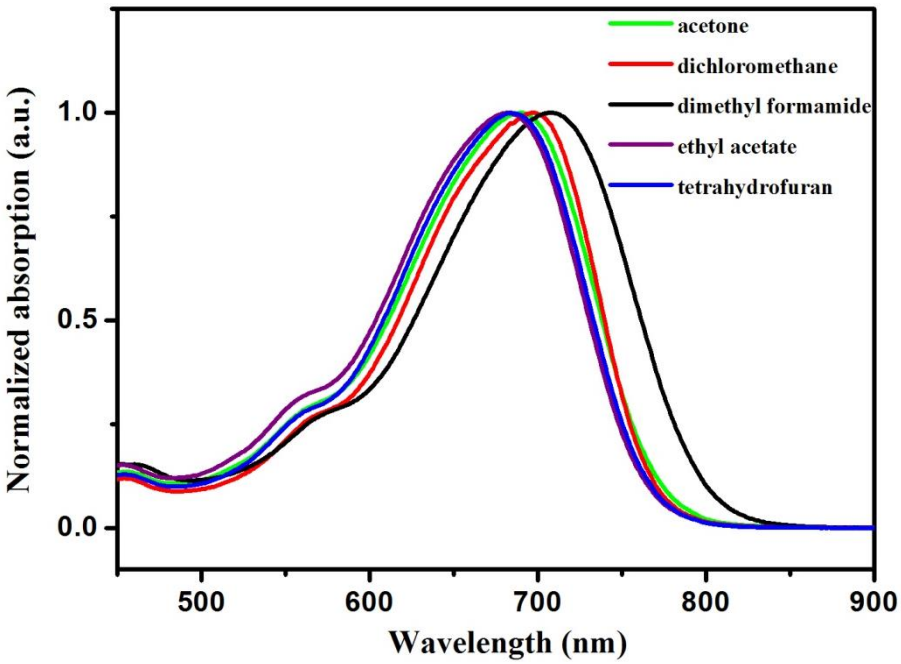

Figure S5. Normalized absorption spectra of PDI in different organic solvents.

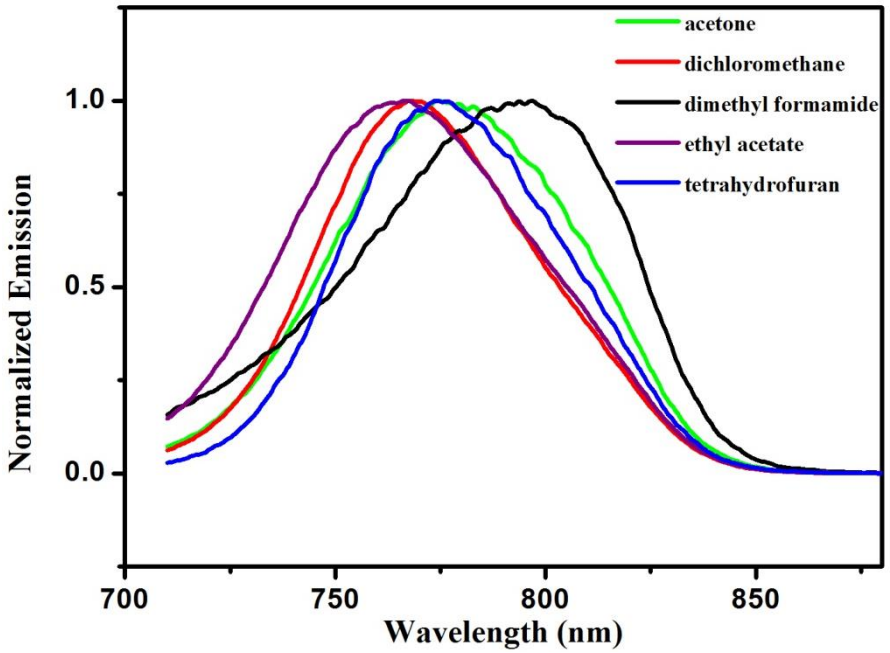

Figure S6. Normalized emission spectra of PDI in different organic solvents.

Table S1. Summary of optical absorption and emission properties of PDI in various organic solvents.

Compound **PDI**	λ_{abs} (nm)/(ε (M^{-1} cm^{-1})[a])	λ_{em}[b] (nm)	ϕ_f (%)
Acetone	689	775	0.56
Dichloromethane	697	768	1.1
Dimethyl Formamide	707	797	0.22
Ethyl acetate	682	767	0.96
Tetrahydrofuran	684	774	0.72

[a]Measured at $2*10^{-5}$ M
[b] λ_{ex} ~ 700 nm

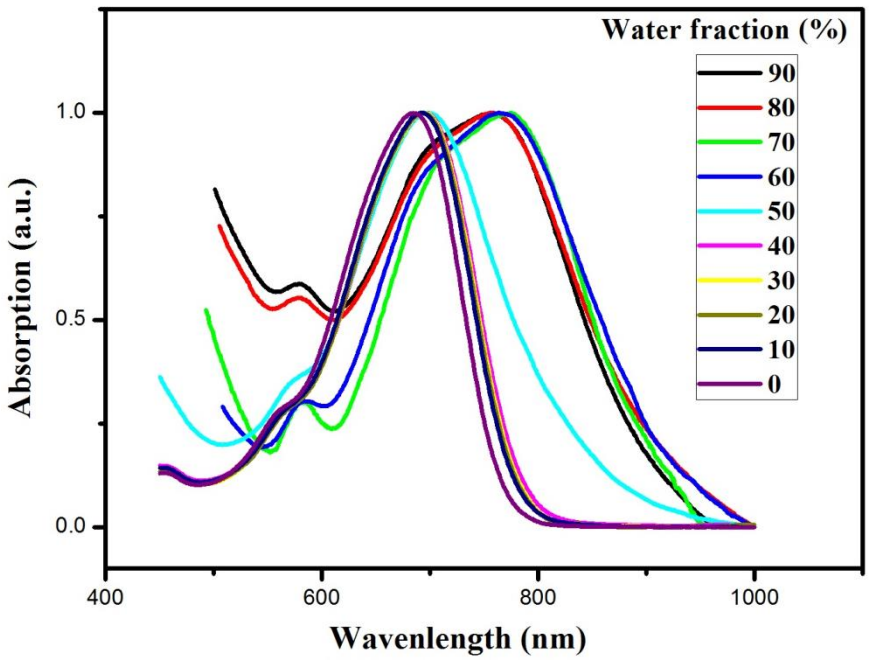

Figure S7. Normalized absorption spectra of PDI in THF/water mixtures with different volume rations

To compare the difference of optical properties between single molecule of PDI dye and PDI NP with aggregated PDI core, the changes of optical properties of PDI molecule in the solvent mixtures of THF(good solvent for PDI) and H_2O (poor solvent for PDI) with different contents were studied. In **Figure S7**, it was showed that when the content of water in the solvent mixture increased, a new red-shifted absorption peak of PDI at around 780 nm formed and gradually increased, indicating the typical π-π intermolecular aggregation of PDI was formed after adding poor solvent into good solvent. Such a red-shift of the new absorption peak, in accordance with the previously reported optical properties of aggregated PDI molecules, was attributed to the planar molecular structure of PDI which could form strong π-π intermolecular aggregation (**ref. 5-6**). Furthermore, a weak fluorescence of PDI was found in THF while no fluorescence existed in THF/water mixture, indicating the formed PDI aggregation could efficiently produce fluorescence quenching which will be beneficial to transfer the excited light energy into PA signals. It was found that all the optical properties of

PDI NP in water were the same as the PDI dye in THF/water mixture, demonstrating the π-aggregated state of PDI molecules dominated in the PDI NPs.

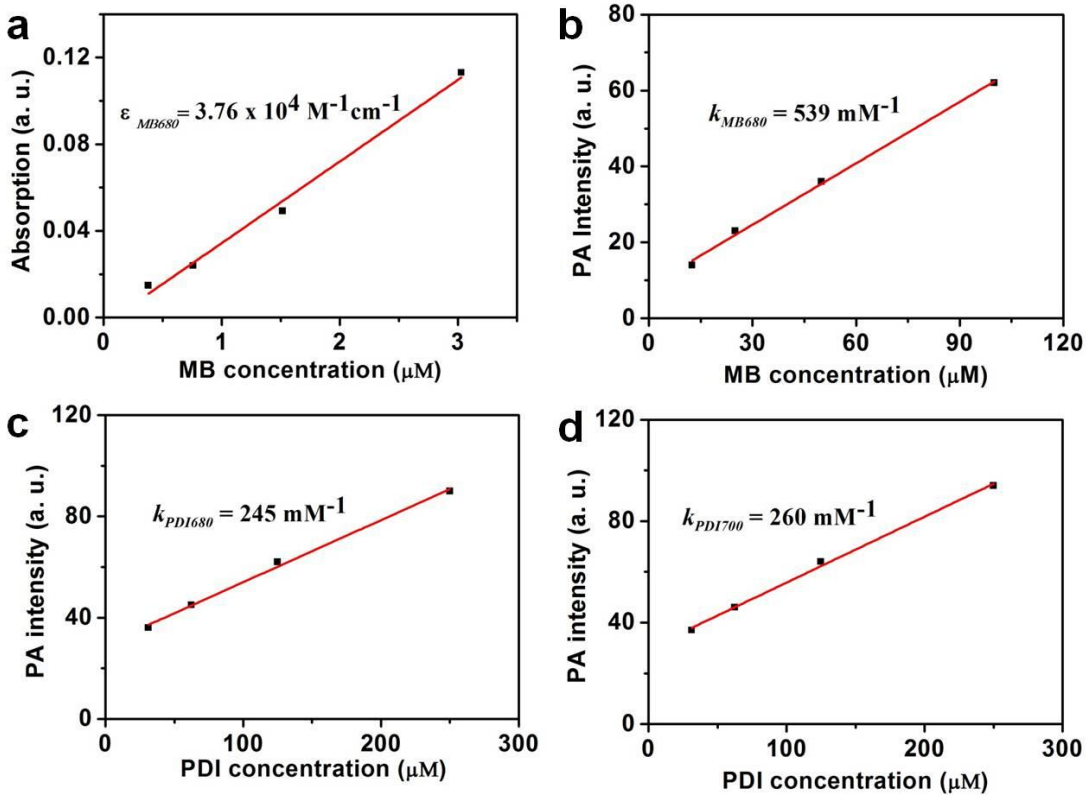

Figure S8. The relationships of UV-vis-NIR absorption of MB with its concentration (a), and the relationship of PA intensity of MB at 680 nm (b), PDI at 680 nm (c) and PDI at 700 nm (d) with their concentrations respectively.

The absorption coefficient of PDI dye in THF at 680 nm was calculated to be 1.84×10^4 $M^{-1}cm^{-1}$. However, the absorption coefficient of PDI NPs in water cannot be directly obtained from the conventional UV−vis−NIR spectrometer because it can only measure the extinction spectra of nanostructures which contains two components: light scattering and light absorption. Combining UV−vis−NIR spectrometer and PA measurements can be used to calculate the absorption coefficient. According to the previously reported method (**ref. 7-8**), methylene blue (MB) with known absorption coefficient was also used as the reference dye to calibrate the absorption coefficient of PDI NPs through the linear relationship between

absorption coefficient (ε) and photoacoustic signal amplitude coefficient (k). The equations are as follows:

$$\text{PA signal} = k \times [\text{M}] + \text{PA}_0 \qquad (1)$$

$$\frac{\varepsilon_{MB680}}{\varepsilon_{PDI\,680}} = \frac{k_{MB680}}{k_{PDI\,680}} \qquad (2)$$

In **Equation 1**, [M] is the concentration of PA contrast agent, PA_0 is the PA signal when [M] = 0, and in **Equation 2** ε_{MB680} is the absorption coefficient of MB at 680 nm, ε_{PDI680} is the absorption coefficient of PDI at 680 nm, k_{MB680} is the PA signal amplitude coefficient of MB at 680 nm, and k_{PDI680} is the PA signal amplitude coefficient of PDI at 680 nm. The PA signal amplitude coefficients of PDI in NPs at 680 nm and MB at 680 nm were obtained from **Figure S8c and S8b** to be 245 mM^{-1} (using PDI molecule as mole number) and 539 mM^{-1} respectively. Considering the absorption coefficient of methylene blue at 680 nm is 3.76×10^4 $M^{-1}cm^{-1}$ (**Figure S8a**), the absorption coefficient of PDI in NPs at 680 nm was calculated from **Equation 2** to be 1.71×10^4 $M^{-1}cm^{-1}$ (using PDI molecule as mole number) which is similar with PDI dye in THF at 680 nm (1.84×10^4 $M^{-1}cm^{-1}$). Thus the optical property per PDI NP appeared the accumulated optical properties of the 10000 PDI molecules in one NP, which exhibited obviously stronger absorption coefficient (1.71×10^8 $M^{-1}cm^{-1}$, using PDI NP as mole number) than separated PDI molecule. Furthermore, because the extinction coefficient of PDI NP at 680 nm is 1.95×10^8 $M^{-1}cm^{-1}$, the scattering coefficient of PDI NP at 680 nm was calculated to be 0.24×10^8 $M^{-1}cm^{-1}$ which is much smaller than its absorption coefficient. Considering the similar extinction coefficients (2.00×10^8 $M^{-1}cm^{-1}$) and PA signal amplitude (260 mM^{-1}) of PDI NP at 700 nm (**Figure S8d**) with that at 680 nm, we can infer that the absorption and PA properties of PDI NP at 700 nm is similar with that at 680 nm.

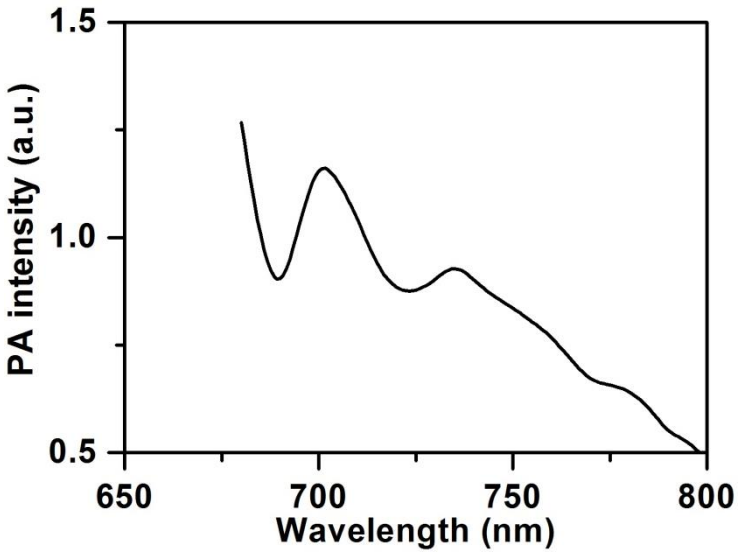

Figure S9. PA spectrum of PDI NP's phantom

The PA spectrum of PDI NP's phantom has been showed in **Figure S9**. From the spectrum, it is clear that the maximum PA signal of PDI NP was at 700 nm, which is the same as the maximum absorption of PDI NP at 700 nm. Thus, 700 nm was selected as the excitaion laser wavelength in our system to obtain good PA signals.

Stability of PDI NP

Generally the NP's hydrodynamic size distribution in serum was measured to evaluate the stability of NPs in the in vivo environments (**ref. 9-10**). The PDI NPs (1 mg) were added to 50% fatal bovine serum (FBS, 5 mL) and 50% PBS (5 mL) and incubated at 37 °C for 48 h. The sample was analyzed at 0 h, 2 h, 4 h, 24 h, and 48 h by dynamic light scattering. Once adding NPs in serum, the hydrodynamic size of the PDI NPs (peaking at 0 h post-incubation at 37 °C) increased to 78 nm, which may be attributed to the association with blood proteins. After 48 h incubation, all the hydrodynamic sizes of PDI NPs still retained at around 78 nm and their polydispersities were not changed. Thus, we concluded that the NPs are stable in serum. (**Figure S10**).

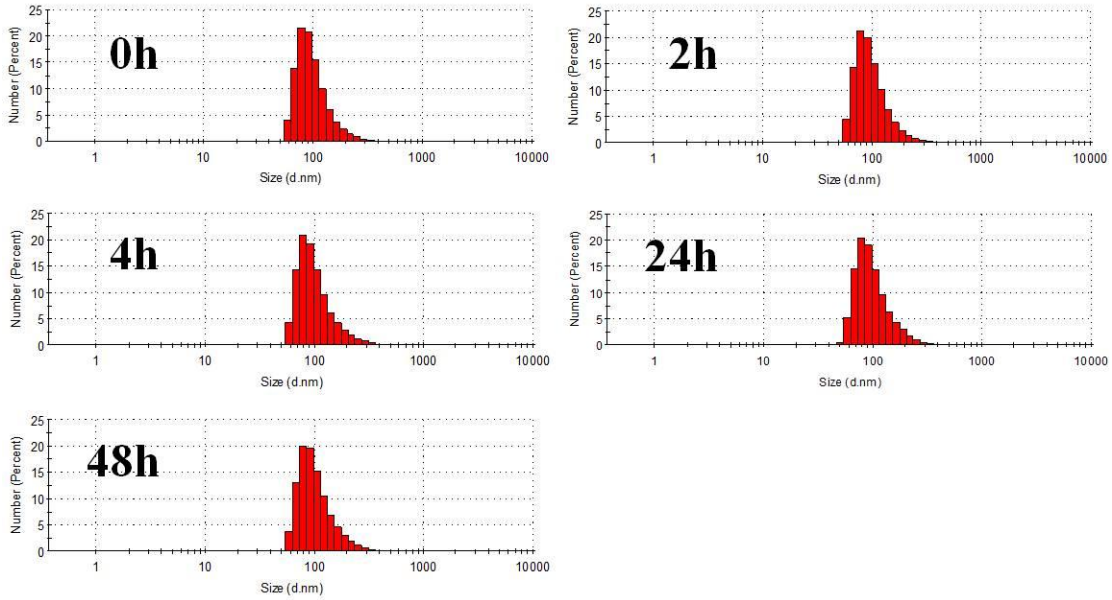

Figure S10. Stability of the PDI NPs hydrodynamic size during different incubation periods with serum.

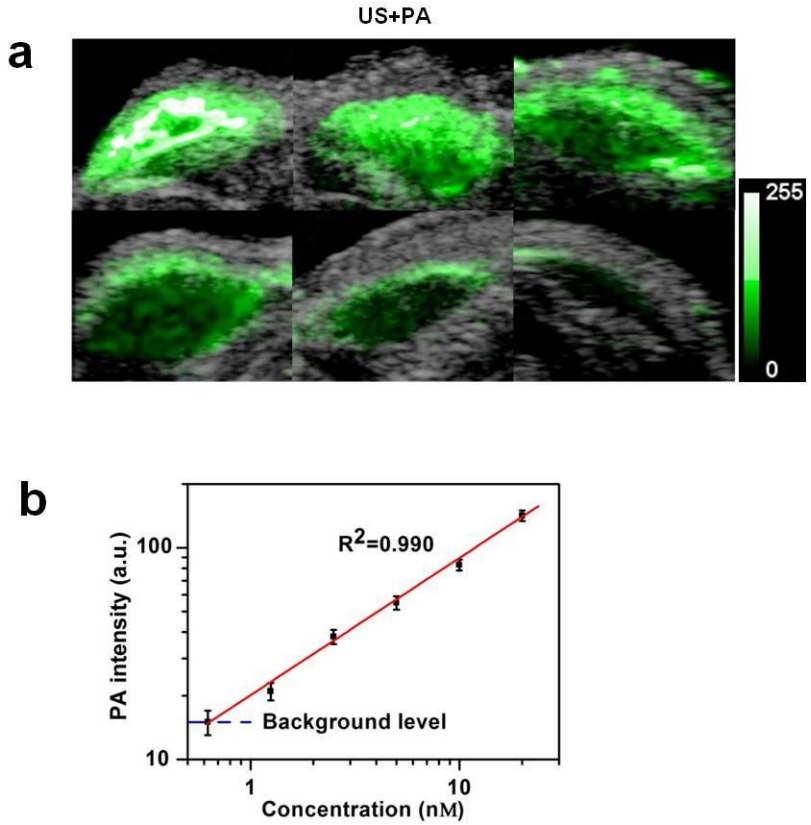

Figure S11. *Phantom* study of PAI of PDI NPs. (a) Photoacoustic detection of PDI NPs in living mice. Mice were injected subcutaneously with PDI NPs at concentrations of 20, 10, 5 (from left to right in top row), and 2.5, 1.25, 0.625 (from left to right in bottom row) nM. One

vertical slice in the photoacoustic image (green) was overlaid on the corresponding slice in the ultrasound image (grey). (b) The photoacoustic signal from each inclusion was calculated. The background level represents the endogenous signal measured from tissues. The linear regression was calculated on the six most concentrated inclusions (R^2 = 0.990).

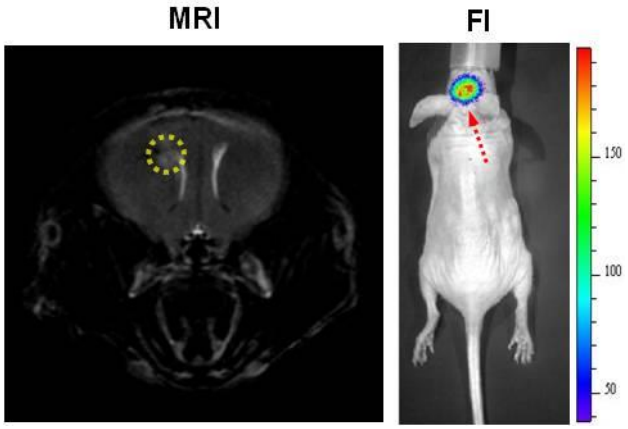

Figure S12. (a) T_2 MRI (left) and BLI (right) of brain tumor in living mice after 18d of tumor cell injection.

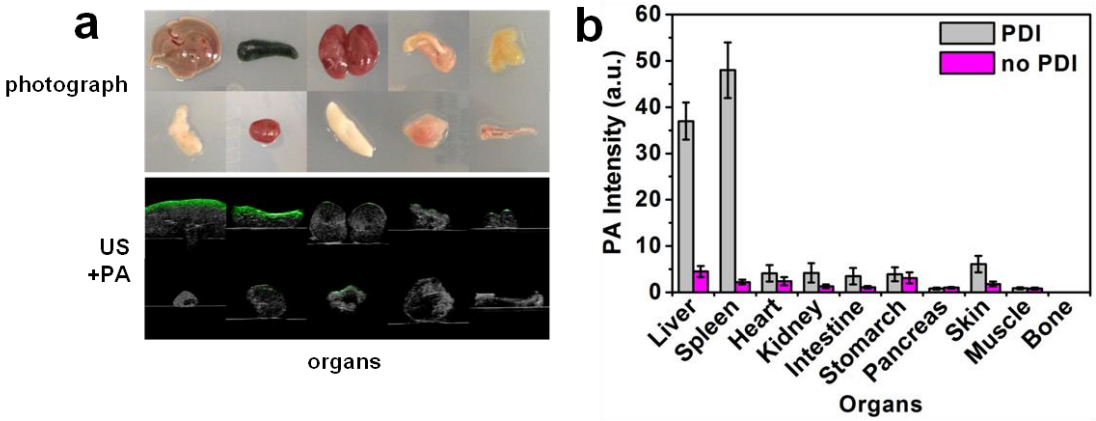

Figure S13. The accumulation of PDI NPs in major organs. (a) photographic image and PA coronal image of major organs collected after 2 day NPs injection. From left to right in the top row: liver, spleen, kidney, stomach, and intestine. From left to right in the bottom row: pancreas, heart, skin, muscle, and bone. (b) the PA signal intensity of major organs after 2 day

NPs injection. The PA signals in major organs showed that most of the PDI NPs accumulated in liver and spleen.

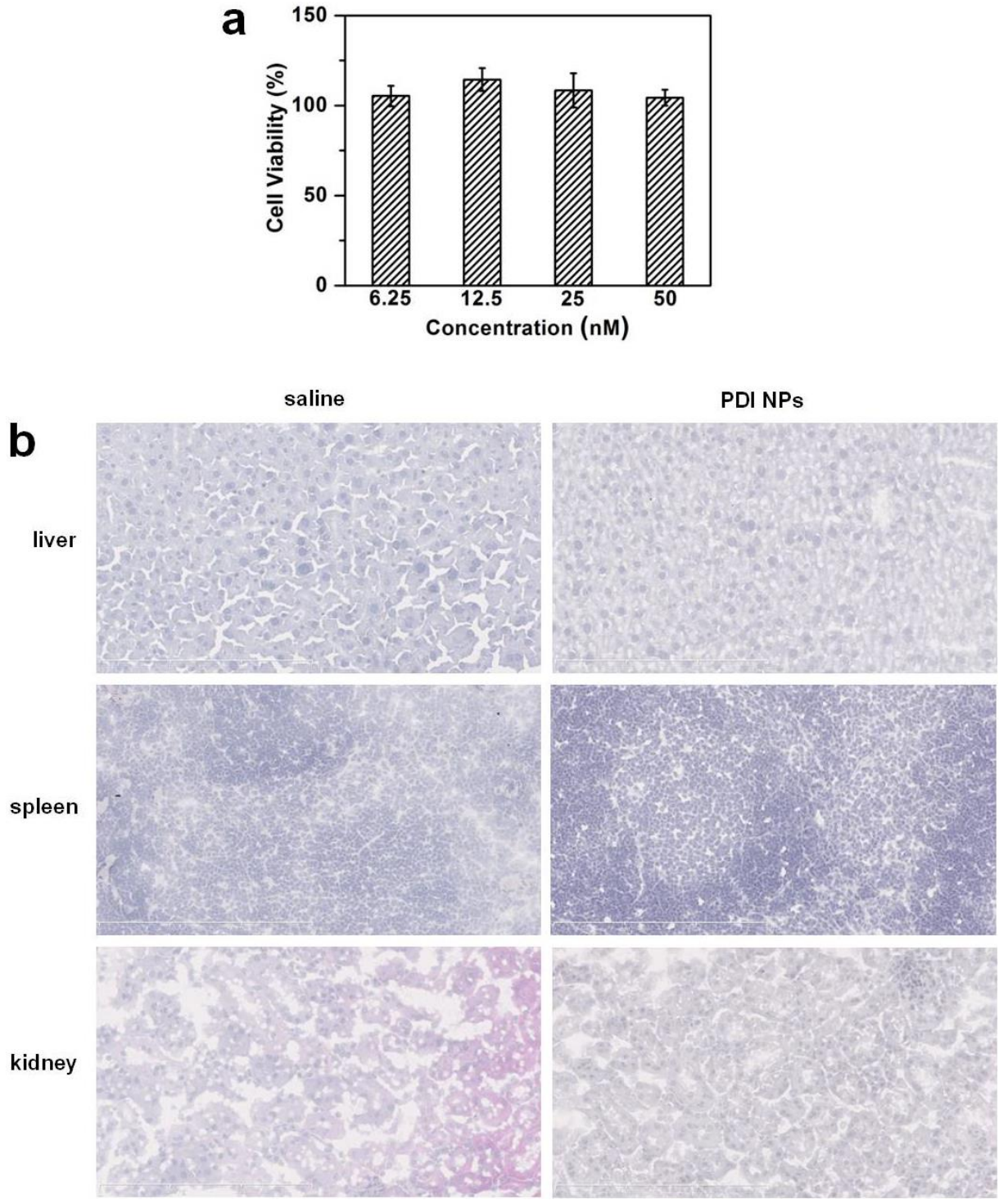

Figure S14. Toxicity evaluation of PDI NPs. (a) MTT assay using NIH-3T3 cells with PDI NPs concentration 6.25, 12.5, 25 and 50 nM after 24 h incubation at 37 °C. (b) Representative haematoxylin and eosin stained sections of liver, spleen, and kidney from mice 7 day after

tail-vein injection of 250 μL of 250 nM PDI NPs. It was showed that no apparent change in cellular structure after 7 day PDI NPs injection.

References

1. F. Würthner, V. Stepanenko, Z. J. Chen, C. R. Saha-Möller, N. Kocher, and D. Stalke, *J. Org. Chem*. **2004**, 69, 7933−7939.

2. C. T. Zhao, Y. X. Zhang, R. J. Li, X. Y. Li, and J. Z. Jiang, *J. Org. Chem.* **2007**, 72, 2402−2410.

3. D. Marsh, R. Bartucci, and L. Sportelli, *Biochim. Biophys. Acta*. **2003**, 1615, 33−59.

4. M. J. Ahrens, M. J. Tauber, and M. R. Wasielewski, *J. Org. Chem.* **2006**, 71, 2107−2114.

5. R. Marty, R. Nigon, D. Leite, and H. Frauenrath, *J. Am. Chem. Soc.* **2014**, 136, 3919−3927.

6. K. Sugiyasu, N. Fujita, and S. Shinkai, *Angew. Chem.* **2004**, 116, 1249−1249.

7. K. Cheng, S-R. Kothapalli, H. G. Liu, A. L. Koh, J. V. Jokerst, H. Jiang, M. Yang, J. B. Li, J. Levi, J. C. Wu, S. S. Gambhir, and Z Cheng, *J. Am. Chem. Soc*. **2014**, 136, 3560−3571.

8. E. C. Cho, C. Kim, F. Zhou ,C. M. Cobley, K. H. Song, J. Y. Chen, Z-Y. Li, L. V. Wang and Y. Xia, *J. Phys. Chem. C.* **2009**, 113, 9023–9028.

9. M. F. Kircher, A. de la Zerda, J. V. Jokerst, C. L. Zavaleta, P. J. Kempen, E. Mittra, K. Pitter, R. Huang, C. Campos, F. Habte, R. Sinclair, C. W. Brennan, I. K. Mellinghoff, E. C. Holland, S. S. Gambhir, *Nat. Mater.* **2012**, *18*, 829–834.

10. K. Pu, A. J. Shuhendler, J. V. Jokerst, J. Mei, S. S. Gambhir, Z. Bao, J. Rao, *Nat. Nanotechnol.* **2014**, *9*, 233–239.